



Unexpected increase in low-temperature NH₃-SCR catalytic activity over Cu-SSZ-39 after hydrothermal aging

Jinpeng Du^{a,b}, Yulong Shan^{a,*}, Yu Sun^{a,b}, Meng Gao^{a,b}, Zhongqi Liu^{a,b}, Xiaoyan Shi^{a,b}, Yunbo Yu^{a,b}, Hong He^{a,b,c,*}

^a State Key Joint Laboratory of Environment Simulation and Pollution Control, Research Center for Eco-Environmental Sciences, Chinese Academy of Sciences, Beijing, 100085, China

^b University of Chinese Academy of Sciences, Beijing, 100049, China

^c Center for Excellence in Regional Atmospheric Environment, Institute of Urban Environment, Chinese Academy of Sciences, Xiamen, 361021, China

ARTICLE INFO

Keywords:

NO_x reduction
NH₃-SCR
Cu-SSZ-39
Hydrothermal aging
Cu_xO_y species

ABSTRACT

The control of nitrogen oxides (NO_x) from heavy-duty diesel vehicles is becoming increasingly urgent due to its detrimental effects on the environment. Cu-SSZ-39, with its exceptional NH₃-SCR activity and hydrothermal stability, has attracted more and more attention in the field of diesel vehicle emission control. In this work, an unexpected phenomenon was observed for Cu-SSZ-39 after hydrothermal aging. Generally, the hydrothermal aging process causes deterioration of the catalytic performance of catalysts. However, a remarkable increase in low-temperature NH₃-SCR catalytic activity was observed in Cu-SSZ-39 after it was exposed to 850 °C hydrothermal aging conditions for 16 h. EPR, DRIFTS, H₂-TPR, UV-vis and XANES were utilized to detect the changes in Cu species. It was determined that a portion of the Cu²⁺ ions near double six-membered rings (d6r) transformed into Cu_xO_y species after hydrothermal treatment. These Cu_xO_y species facilitated the production of nitrate species which were critical intermediates in the NH₃-SCR process, resulting in an increase in low-temperature catalytic activity.

1. Introduction

Nitrogen oxide (NO_x) emissions from heavy-duty diesel vehicles contribute extensively to air pollution problems. Selective catalytic reduction of NH₃ (NH₃-SCR) has been considered the dominant technology for NO_x control in diesel vehicles [1]. Apart from the abatement of NO_x, the elimination of particulate matter (PM) is also crucial. A diesel particulate filter (DPF) is used for the removal of PM; however, high-temperature regeneration is frequently needed for the combustion of PM. Therefore, SCR catalysts are often exposed to high temperature and humid conditions, resulting in a requirement of high hydrothermal stability for SCR catalysts [2]. Cu-SSZ-39, a newly studied zeolite developed in the past 10 years, is known for its excellent hydrothermal stability [3]. Meanwhile, it also possesses good NH₃-SCR activity, N₂ selectivity and sulfur tolerance [4,5]. As a result, it is becoming one of the most promising commercial catalysts in NO_x control systems of heavy-duty diesel vehicles.

In general, the high-temperature hydrothermal aging process always

induces a decline in NH₃-SCR activity [6,7]. Hydrothermal treatment can cause the loss of active Cu ions, resulting in a decrease in catalytic activity. In the meantime, the accumulated Cu_xO_y species would also cause a decline in NO_x conversion at high temperatures due to non-selective oxidation of NH₃ [8,9]. Meanwhile, collapse of the skeleton also leads to the loss of Brønsted acid sites, which act as a NH₃ reservoir as well as active centers in some specific circumstances [10,11]. Furthermore, the aggregation of copper ions and the collapse of the framework feed off each other [7,12]. Nam et al. found that the motion of Cu_xO_y clusters inside zeolite pore channels accelerated the deterioration of the framework [7]. At the same time, Cu ions are more likely to accumulate into Cu_xO_y clusters due to a deficiency in ion-exchanged sites [9,13]. As a result, the loss of active Cu ions and Brønsted acid sites together with the formation of Cu_xO_y species cause a decrease in catalytic activity in many small pore zeolites.

However, there has been an abnormal phenomenon occurring in some specific small pore zeolites after high-temperature hydrothermal treatment. It was observed by many researchers that catalytic activity

* Corresponding authors at: State Key Joint Laboratory of Environment Simulation and Pollution Control, Research Center for Eco-Environmental Sciences, Chinese Academy of Sciences, Beijing, 100085, China.

E-mail addresses: ylshan@ceees.ac.cn (Y. Shan), honghe@ceees.ac.cn (H. He).

<https://doi.org/10.1016/j.apcatb.2021.120237>

Received 12 January 2021; Received in revised form 21 March 2021; Accepted 15 April 2021

Available online 19 April 2021

0926-3373/© 2021 Elsevier B.V. All rights reserved.

was improved in Cu-SAPO-34 after high-temperature hydrothermal aging [14,15]. After a comparison of Cu species in the fresh and aged Cu-SAPO-34, the transformation of Cu_xO_y species into active Cu^{2+} was thought to be the cause of this phenomenon [15,16]. Hong et al. found that the catalytic performance of aged LTA zeolites was better than that of fresh ones. With investigation of the precise position of Cu ions, it was found that Cu ions migrated from inert sites to active sites during the hydrothermal aging process [17,18]. Furthermore, an increase in NO conversion was also observed by Sonoda et al. in P-modified Cu-SSZ-39 after hydrothermal aging at 900 °C; however, they did not pay much attention to the phenomenon [19].

In this study, we also observed an increase in the low-temperature catalytic activity of Cu-SSZ-39 after hydrothermal aging. EPR, DRIFTS, H_2 -TPR, UV-vis and XANES were carried out to examine the changes in Cu species. As a result, it was inferred that the formation of Cu_xO_y species was the cause of the increased low-temperature catalytic activity. Moreover, we proved that Cu_xO_y species were SCR-active in Cu-SSZ-39, and the reaction process was investigated with the help of *in situ* DRIFTS. The results of this study not only contributed to knowledge on Cu-SSZ-39 catalysts, but also brought us better understanding of the function of Cu_xO_y species in NH_3 -SCR.

2. Experimental

2.1. Catalyst preparation

The Cu-SSZ-39 catalysts were prepared by a hydrothermal method using N, N-dimethyl-3, 5-dimethylpiperidinium as structure directing agent (SDA). The initial ratio of materials was as follows: 3 g Y zeolite: 4.5 g SDA (25 wt. %): 25.5 g H_2O : 0.75 g NaOH, and the following procedure was the same as described in the literature [4]. The elemental composition was detected by Inductively Coupled Plasma Optical Emission Spectrometry (ICP-OES). Cu-SSZ-39 catalysts with Si/Al ratio of 6.8, and Cu loading of 0.5 %, 1.3 %, 1.8 %, 2.0 % and 2.3 % (Cu/Al: 0.05, 0.13, 0.17, 0.2, 0.23) were obtained by ion-exchange of NH_4 -SSZ-39 with 0.001 M, 0.005 M, 0.01 M, 0.05 M and 0.2 M Cu (NO_3)₂, respectively. The Cu-SSZ-39 catalysts with different Cu loading were denoted as $\text{Cu}_{0.5}$ -SSZ-39-fresh, $\text{Cu}_{1.3}$ -SSZ-39-fresh, $\text{Cu}_{1.8}$ -SSZ-39-fresh, $\text{Cu}_{2.0}$ -SSZ-39-fresh and $\text{Cu}_{2.3}$ -SSZ-39-fresh. 200 mg of the fresh catalysts were placed in quartz tubes with quartz wool blocking both ends, so that gas can pass through the catalysts. The catalysts were hydrothermally treated in 10 % H_2O /air at 850 °C for 16 h (ramp rate: 10 °C/min), with a total gas flow of 200 mL/min, and then cooled naturally to room temperature after aging. The aged catalysts were denoted as $\text{Cu}_{0.5}$ -SSZ-39-HTA, $\text{Cu}_{1.3}$ -SSZ-39-HTA, $\text{Cu}_{1.8}$ -SSZ-39-HTA, $\text{Cu}_{2.0}$ -SSZ-39-HTA and $\text{Cu}_{2.3}$ -SSZ-39-HTA, respectively. Furthermore, to prepare catalysts with various Cu_xO_y contents, we treated $\text{Cu}_{1.8}$ -SSZ-39-fresh at various temperatures. The aging conditions were the same as those for the hydrothermal aging process at 850 °C; however, the temperatures were set at 650 °C, 675 °C, 700 °C, and 750 °C, and the aging time was set at 2 h. In the meantime, we tried to dissolve some of the Cu_xO_y species in $\text{Cu}_{1.8}$ -SSZ-39-HTA to further confirm the function of the Cu_xO_y species. 500 mg $\text{Cu}_{1.8}$ -SSZ-39-HTA catalyst was dissolved into 50 ml HNO_3 with a concentration of 0.01 M. After stirring for 5 h at 40 °C, the solution was dried by rotary evaporation. The obtained powder was dried at 100 °C overnight for further characterization.

2.2. Catalyst characterization

ICP-OES with a PerkinElmer OPTIMA 8300 spectrometer was used to detect the concentration of elements in the catalysts. X-Ray diffraction (XRD) was carried out on a Bruker D8 ADVANCE diffractometer with Cu $\text{K}\alpha$ radiation ($\lambda = 0.15406$ nm). Magnetic Angle Spinning Nuclear Magnetic Resonance (MAS NMR) spectra were utilized to detect the coordination environment of framework atoms. ^{27}Al NMR and ^{29}Si NMR

signals were detected by a 3.2 mm CP MAS probe with relaxation times of 5 s and 8 s, respectively, and the mass frequency was 12 kHz.

Electron paramagnetic resonance (EPR) was used to detect Cu ions, and the experiment was carried out on a Bruker E500 X-band spectrometer at -120 °C. *In situ* DRIFTS of NH_3 adsorption was carried out to distinguish Cu ions, and the experiments were carried out on a Thermo Nicolet IS50 with MCT/A detector. The catalysts were pretreated at 500 °C under 20 % O_2/N_2 for 30 min, and after the temperature was reduced to 200 °C, 500 ppm NH_3/N_2 was introduced. The redox properties of the catalysts were tested by temperature programmed reduction of H_2 (H_2 -TPR) experiments on a Micromeritics AutoChem 2920 chemisorption analyzer. The catalysts were pretreated at 500 °C under 20 % O_2/N_2 for 1 h, and the reduction process was carried out under 10 % H_2/Ar from 50 °C to 800 °C at a ramp rate of 10 °C/min. Ultraviolet visible diffuse reflectance spectroscopy (UV-vis-DRS) was carried out on a Varian Cary 5000 spectrometer at room temperature with scanning range from 20,000 cm^{-1} to 50,000 cm^{-1} . X-ray absorption near edge structure (XANES) spectra were used to detect the coordination environment of Cu, and the experiment was carried out in the 1W1B beamline of Beijing Synchrotron Radiation Facility. Transmission electron microscopy (TEM) was employed to observe the formation of Cu_xO_y clusters after hydrothermal aging, using a Double Aberration-Corrected TEM (Titan Cubed Themis G2 300).

In situ DRIFTS was used to investigate the NH_3 -SCR mechanism over catalysts. All the catalysts were pretreated by the same procedure as the NH_3 adsorption experiment, and the reaction temperature was set at 200 °C. To investigate the reaction of $\text{NO} + \text{O}_2$ with adsorbed NH_3 , catalysts were exposed under 500 ppm NH_3 until saturated, and purged by N_2 for 1 h before 500 ppm NO and 5% O_2 were added. The same procedure was carried out but $\text{NO} + \text{O}_2$ was added firstly, followed by NH_3 introduced after N_2 purging to investigate the reaction of adsorbed nitrate species with NH_3 . The spectra with a resolution of 4 cm^{-1} was recorded throughout the whole process by accumulation of 100 scans.

2.3. NH_3 -SCR, NO/NH_3 oxidation activity and dynamic tests

The NH_3 -SCR activity test was carried out in a fixed-bed reactor heated by a tube furnace. The composition of the inlet gas was: $[\text{NO}] = [\text{NH}_3] = 500$ ppm, $[\text{O}_2] = [\text{H}_2\text{O}] = 5$ %, balanced by N_2 . The catalysts were screened to 40–60 mesh before being sealed with quartz wool in a quartz tube. The total gas flow was 500 ml/min with the GHSV = 400,000 h^{-1} . The outlet gas was detected by an online Nicolet IS10 spectrometer, and the NO_x conversion was calculated by the following equation:

$$\text{NO}_x \text{ conversion} = \left(1 - \frac{[\text{NO}_x]_{\text{out}}}{[\text{NO}_x]_{\text{in}}} \right) \times 100\% \quad (\text{NO}_x = \text{NO} + \text{NO}_2)$$

A NO oxidation experiment was carried out by the same procedure as the NH_3 -SCR experiment; however, the composition of the inlet gas was: $[\text{NO}] = 500$ ppm, $[\text{O}_2] = 5$ %, balanced by N_2 . The NO conversion was calculated by the following equation:

$$\text{NO conversion} = \left(1 - \frac{[\text{NO}]_{\text{out}}}{[\text{NO}]_{\text{in}}} \right) \times 100\%$$

An NH_3 oxidation experiment was also conducted by the same procedure as the NH_3 -SCR and NO oxidation experiments, with the composition of the inlet gas: $[\text{NH}_3] = 500$ ppm, $[\text{O}_2] = 5$ %, balanced by N_2 . The NH_3 conversion was calculated by the following equation:

$$\text{NH}_3 \text{ conversion} = \left(1 - \frac{[\text{NH}_3]_{\text{out}}}{[\text{NH}_3]_{\text{in}}} \right) \times 100\%$$

Meanwhile, the reaction rate was calculated by the equation below, where F is the flow rate of NO_x (mol/s), w is the mass of catalyst (g), and x is NO_x conversion. The Standard SCR rate was calculated by this equation.

$$r = \frac{F}{w} (-\ln(1-x))$$

3. Results

3.1. Catalytic performance

3.1.1. NH_3 -SCR activity test

The NH_3 -SCR test was carried out on the fresh and hydrothermally aged catalysts, and the standard SCR rate of catalysts with moderate Cu content was calculated and summarized in Fig. 1. For the fresh catalysts, the standard SCR rate rose with the increase of Cu loading over the whole temperature range. Meanwhile, there was a decline in the standard SCR rate around 350 °C. This so-called “seagull shape” profile was also observed in the studies of Cu-SSZ-13 [20,21]. After hydrothermal aging at 850 °C for 16 h, there was a remarkable increase in the standard SCR rate below 400 °C for all three catalysts; meanwhile, all aged catalysts presented a decline in the standard SCR rate over 450 °C. To find out the cause of this abnormal phenomenon, $\text{Cu}_{1.8}$ -SSZ-39-fresh and $\text{Cu}_{1.8}$ -SSZ-39-HTA were chosen to carry out further investigations. Furthermore, the results were different when the Cu content was too high or too low. The standard SCR rates of the fresh and aged catalysts with Cu content of 0.5 % and 2.3 % are presented in Fig. S1. When the Cu content was 0.5 %, no “seagull shape” profile could be observed, indicating that the reaction mechanism could be different. Meanwhile, the standard SCR rate for both $\text{Cu}_{0.5}$ -SSZ-39-HTA and $\text{Cu}_{2.3}$ -SSZ-39-HTA was lower than that of $\text{Cu}_{0.5}$ -SSZ-39-fresh and $\text{Cu}_{2.3}$ -SSZ-39-fresh. Further analysis of this interesting phenomenon will be included in the following sections.

3.1.2. NO and NH_3 oxidation test

NO oxidation and NH_3 oxidation experiments were conducted, and the profiles are presented in Fig. S2. In the temperature range from 150 °C to 300 °C, only slight conversion of NO was observed in both $\text{Cu}_{1.8}$ -SSZ-39-fresh and $\text{Cu}_{1.8}$ -SSZ-39-HTA. This result indicates that NO cannot be oxidized into NO_2 on either the fresh or aged catalysts, which rules out the possibility that the formation of NO_2 in the aged catalyst facilitates NO_x conversion through the fast SCR process. In addition, the NH_3 oxidation profiles are depicted in Fig. S2(b). Hardly any conversion of NH_3 was observed for $\text{Cu}_{1.8}$ -SSZ-39-fresh from 150 °C to 550 °C. However, the conversion of NH_3 for $\text{Cu}_{1.8}$ -SSZ-39-HTA became noticeable when the temperature was higher than 275 °C, especially in the high-temperature range (over 450 °C). It has been reported that Cu_xO_y species in small-pore zeolites can facilitate NH_3 oxidation in the high-

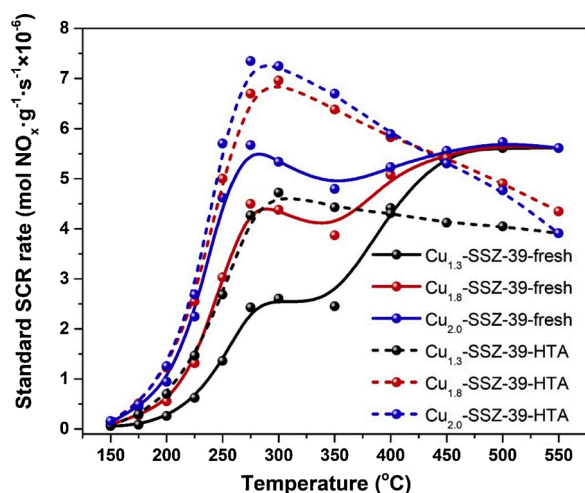


Fig. 1. NH_3 -SCR activity of fresh and hydrothermally aged catalysts with Cu contents of 1.3 %, 1.8 % and 2.0 %.

temperature range, resulting in a decrease in NH_3 -SCR activity due to a shortage of NH_3 [8,9]. Therefore, the decrease in the SCR rate at high temperature in the Cu -SSZ-39-HTA catalysts could be due to the existence of Cu_xO_y species. However, further investigations were still needed.

3.2. Changes in the framework

To investigate the difference in the framework between the fresh and the aged catalysts, XRD and NMR were carried out. The XRD patterns of $\text{Cu}_{1.8}$ -SSZ-39-fresh and $\text{Cu}_{1.8}$ -SSZ-39-HTA are presented in Fig. 2. As can be seen, $\text{Cu}_{1.8}$ -SSZ-39-fresh showed the XRD pattern of the AEI structure with good crystallinity. To calculate the change in the crystallinity of the catalysts after hydrothermal aging, the peak intensities at 17.3°, 20.8°, 21.5°, 24.1° and 31.4° of $\text{Cu}_{1.8}$ -SSZ-39-fresh and $\text{Cu}_{1.8}$ -SSZ-39-HTA were compared. It was found that the crystallinity of the aged catalyst decreased by ~8% compared to the fresh one, which indicated that the long-range order of the catalyst was hardly affected by hydrothermal treatment. To further investigate changes in the coordination environment of Si and Al, ²⁷Al NMR and ²⁹Si NMR experiments were carried out, and the results are presented in Fig. 3(a) and (b), respectively. In the ²⁷Al NMR profile, the chemical shifts at 63 ppm and 4 ppm were assigned to the response of tetrahedral Al atoms and octahedral Al atoms, respectively. As can be seen, most of the framework Al are tetrahedrally coordinated in all catalysts. A peak for extra-framework octahedral Al atoms (~4 ppm) can be seen in H-SSZ-39 and $\text{Cu}_{1.8}$ -SSZ-39-fresh, and the intensity of the peak at 4 ppm is higher in H-SSZ-39 than in $\text{Cu}_{1.8}$ -SSZ-39-fresh, indicating that the ion-exchange process might wash off some extra-framework Al atoms, and the paramagnetic nature of Cu ions may also result in a decrease in this peak. However, there was no peak around 4 ppm observed in the ²⁷Al NMR spectrum of $\text{Cu}_{1.8}$ -SSZ-39-HTA. There could be two reasons: 1. The framework of Cu-SSZ-39 is reconstructed under the hydrothermal aging process, and the extra-framework Al atoms come into the framework of Cu-SSZ-39. 2. Some CuAlO_x species form, resulting in the disappearance of extra-framework Al atoms. In the ²⁹Si NMR profile, the chemical shifts at -104 ppm and -110 ppm were assigned to the response of Si(1Al) and Si(0Al) species, representing the Si atoms surrounded by 4 Si atoms or 3 Si & 1 Al atoms, respectively. The ratio of Si(1Al) atoms is 22 %, 25 % and 14 % in H-SSZ-39, $\text{Cu}_{1.8}$ -SSZ-39-fresh and $\text{Cu}_{1.8}$ -SSZ-39-HTA, respectively. The lower amount of Si atoms surrounded by 3 Si & 1 Al in the aged catalysts indicates that dealumination took place. Combining the results of ²⁷Al NMR and ²⁹Si NMR, we know that dealumination takes place in $\text{Cu}_{1.8}$ -SSZ-39-HTA, and the absence of the peak of octahedral Al is probably due to the formation of some CuAlO_x species

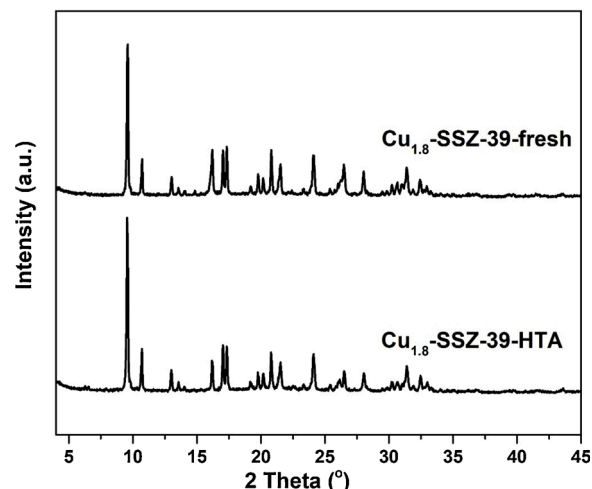


Fig. 2. XRD patterns of $\text{Cu}_{1.8}$ -SSZ-39-fresh and $\text{Cu}_{1.8}$ -SSZ-39-HTA.

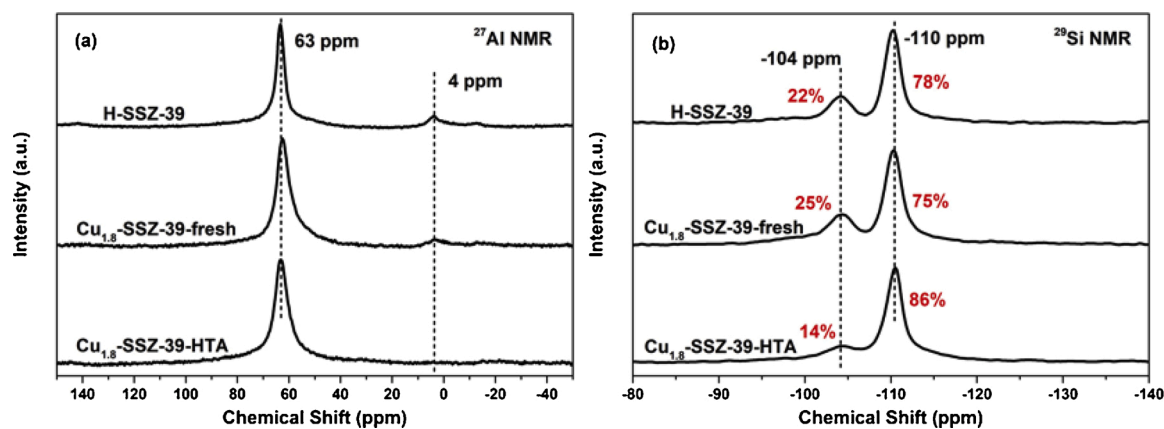


Fig. 3. (a) ^{27}Al NMR and (b) ^{29}Si NMR profiles of $\text{Cu}_{1.8}\text{-SSZ-39-fresh}$ and $\text{Cu}_{1.8}\text{-SSZ-39-HTA}$.

3.3. Changes in Cu species

An EPR experiment was conducted to detect the coordination environment of the Cu ions in the catalysts. As presented in Fig. 4, both $\text{Cu}_{1.8}\text{-SSZ-39-fresh}$ and $\text{Cu}_{1.8}\text{-SSZ-39-HTA}$ showed fourfold split hyperfine spectra with $g_{\parallel} = 2.40$ and $A_{\parallel} = 131$ G, which were assigned to the Cu^{2+} species in d6r [7,22]. This result indicated that only one kind of EPR-active Cu^{2+} ion was observed in both the fresh and the aged catalyst, and that the coordination environment of Cu^{2+} ions did not change after hydrothermal aging. However, 39% of Cu^{2+} ions transformed into EPR-silent copper species in $\text{Cu}_{1.8}\text{-SSZ-39-HTA}$, calculated by second-order integration of the EPR spectra, compared to $\text{Cu}_{1.8}\text{-SSZ-39-fresh}$. Furthermore, Cu ions have an effect on the T—O—T atom vibration in zeolite, which would be influenced by NH_3 solvated Cu^{2+} , resulting in a change in the T—O—T vibration. Therefore, $\text{NH}_3\text{-DRIFTS}$ is often chosen as a reliable means to investigate the locations of Cu ions. As can be seen in Fig. S3, only one negative peak at ~ 900 cm^{-1} was observed in both $\text{Cu}_{1.8}\text{-SSZ-39-fresh}$ and $\text{Cu}_{1.8}\text{-SSZ-39-HTA}$, indicating that Cu^{2+} species near d6r was the only form of Cu ions, which was in accordance with the results of EPR [3,23]. Compared with $\text{Cu}_{1.8}\text{-SSZ-39-fresh}$, the intensity of the negative peak for $\text{Cu}_{1.8}\text{-SSZ-39-HTA}$ was lower. The conclusion can be drawn from the results of EPR and $\text{NH}_3\text{-DRIFTS}$ that Cu^{2+} ions near d6r were the only species in fresh catalysts, and that the amount of these species decreased after hydrothermal aging.

A $\text{H}_2\text{-TPR}$ experiment was further carried out to investigate the changes in Cu species in the fresh and the aged catalysts, and the results

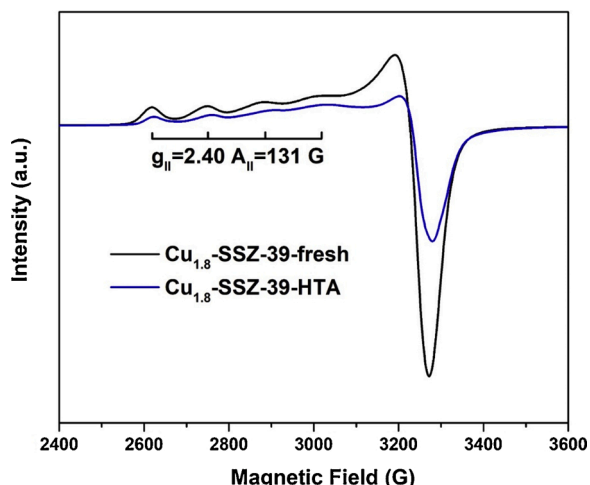


Fig. 4. EPR profiles of $\text{Cu}_{1.8}\text{-SSZ-39-fresh}$ and $\text{Cu}_{1.8}\text{-SSZ-39-HTA}$.

are presented in Fig. 5. Peak A and peak B in $\text{Cu}_{1.8}\text{-SSZ-39-fresh}$ and $\text{Cu}_{1.8}\text{-SSZ-39-HTA}$ were assigned to the reduction of Cu^{2+} to Cu^+ and Cu^+ to Cu^0 , respectively [24,25]. However, the reduction temperature in $\text{Cu}_{1.8}\text{-SSZ-39-HTA}$ was lower than that in $\text{Cu}_{1.8}\text{-SSZ-39-fresh}$. A similar phenomenon was also reported in a previous study, in which we attributed to dealumination of the framework [26]. As we mentioned in the discussion on the ^{29}Si NMR result, dealumination took place after hydrothermal aging, and the restrictive effect of the framework on Cu ions could be weakened, causing Cu ions to be more easily reduced. Furthermore, two new peaks emerged for $\text{Cu}_{1.8}\text{-SSZ-39-HTA}$. Peak C centered around 200–250 $^{\circ}\text{C}$ was attributed to the reduction of Cu_xO_y species [24,25,27]; peak D was assigned to the reduction of Cu^+ to Cu^0 , however, these Cu^+ species were located in more stable sites [28,29]. The relative H_2 consumption of different Cu species was calculated, with the total amount of H_2 consumed by $\text{Cu}_{1.8}\text{-SSZ-39-fresh}$ taken as 1, and the results are presented in Fig. S4. In the results for $\text{Cu}_{1.8}\text{-SSZ-39-fresh}$, the relative amount of H_2 consumed by the reduction of Cu^{2+} to Cu^+ is 60.5%, and it is 39.5% for the reduction of Cu^+ to Cu^0 . This result indicates there are Cu^+ species in more stable locations and they cannot be reduced at temperatures lower than 900 $^{\circ}\text{C}$. In $\text{Cu}_{1.8}\text{-SSZ-39-HTA}$, the relative amount of H_2 consumed by the transformation of Cu^{2+} to Cu^+ is 37.2%. Compared to the fresh catalyst, 39% of Cu^{2+} ions were lost, and this is in accordance with the EPR result that 39% of Cu^{2+} ions were lost after hydrothermal aging. Meanwhile, 14.9% of the H_2 was consumed by Cu_xO_y species. A UV–vis experiment was carried out to investigate the coordination environment of Cu, and the results are presented in Fig. S5. To better compare the difference between the fresh and aged catalysts, we subtracted the intensity of $\text{Cu}_{1.8}\text{-SSZ-39-fresh}$ from that of $\text{Cu}_{1.8}\text{-SSZ-39-HTA}$, and the obtained profile is also given in Fig. S5. The

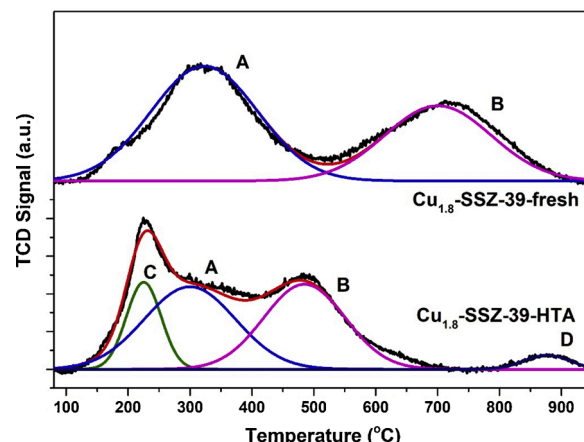


Fig. 5. $\text{H}_2\text{-TPR}$ profiles of $\text{Cu}_{1.8}\text{-SSZ-39-fresh}$ and $\text{Cu}_{1.8}\text{-SSZ-39-HTA}$.

signal around 48300 cm^{-1} was assigned to the ligand-to-metal charge transfer (LMCT) from O^{2-} to Cu^{2+} (or Al^{3+}) of isolated Cu^{2+} [30,31]. The broad peak between $30,000$ and $45,000\text{ cm}^{-1}$ was due to the electron transfer between O and Cu in Cu_xO_y species. However, we still cannot differentiate whether these Cu_xO_y species is CuO or Cu_2O from H_2 -TPR and UV-vis results. XANES spectra of $\text{Cu}_{1.8}\text{-SSZ-39-fresh}$ and $\text{Cu}_{1.8}\text{-SSZ-39-HTA}$ are depicted in Fig. 6, with Cu_2O and CuO as references. The adsorption of energy at 8985 and 8987 eV was assigned to the $1s \rightarrow 4p_{xy}$ electronic transition of Cu^+ in Cu_2O and $1s \rightarrow 4p_z$ electronic transition of Cu^{2+} in CuO, respectively [7,32]. Compared to $\text{Cu}_{1.8}\text{-SSZ-39-fresh}$, the adsorption of energy around 8985 eV and 8987 eV was stronger in $\text{Cu}_{1.8}\text{-SSZ-39-HTA}$, indicating that there was a mixture of Cu_2O and CuO species in the aged catalyst. To quantify the amounts of different Cu species in $\text{Cu}_{1.8}\text{-SSZ-39-HTA}$, we deconvoluted the XANES data. We took Cu_2O , CuO and $\text{Cu}_{1.3}\text{-SSZ-39-fresh}$ as references, and found that 84 % of the Cu species was Cu^{2+} , 14 % was CuO and 2 % was Cu_2O in $\text{Cu}_{1.8}\text{-SSZ-39-HTA}$. As we mentioned in the discussion on H_2 -TPR results, in the aged catalyst, 14.9 % of the relative H_2 amount is consumed by Cu_xO_y species, and 37.2 % of H_2 is consumed by the reduction of Cu^{2+} to Cu^+ . This result means that if the total amount of H_2 consumed by Cu_xO_y and Cu^{2+} is taken as 100%, so that 29 % of H_2 is consumed by Cu_xO_y species and 71 % of H_2 is consumed by Cu^{2+} in $\text{Cu}_{1.8}\text{-SSZ-39-HTA}$. 1 mol of CuO and Cu_2O can consume 1 mol of H_2 , and the reduction of 2 mol of Cu^{2+} to Cu^+ consumes 0.5 mol of H_2 . From the result of XANES, we know that 84 %, 14 % and 2 % of Cu species are Cu^{2+} , CuO and Cu_2O in $\text{Cu}_{1.8}\text{-SSZ-39-HTA}$, respectively. Thus in theory, 26 % of H_2 should be consumed by Cu_xO_y species, and 74 % of H_2 should be consumed by Cu^{2+} ions. This number is quite close to the results we calculated from H_2 -TPR showing that 29 % of H_2 is consumed by Cu_xO_y species and 71 % by Cu^{2+} . Based on the results of H_2 -TPR, UV-vis and XANES, it can be concluded that Cu_xO_y species emerged after hydrothermal aging. In summary, from the investigation of Cu species, we can conclude that after the hydrothermal aging process, some Z_2Cu^{2+} near d_{6r} transformed into Cu_xO_y species. The formation of these Cu_xO_y species might facilitate the standard SCR rate of Cu-SSZ-39. However, further analysis will be included in the following sections.

TEM was used to observe Cu_xO_y species in the aged catalysts, and the results are presented in Fig. 7. It can be seen from Fig. 7(a) that the pores and channels of $\text{Cu}_{1.8}\text{-SSZ-39-fresh}$ are arranged in a rather regular order. After hydrothermal aging at $850\text{ }^\circ\text{C}$, several light spots emerged in the images of $\text{Cu}_{1.8}\text{-SSZ-39-HTA}$, and these spots are believed to be Cu_xO_y clusters. The size of these Cu_xO_y clusters is around $1\text{--}3\text{ nm}$. The dimensions of AEI cages are 13.7 \AA , 12.6 \AA and 18.5 \AA , which means that the size of these Cu_xO_y clusters might be larger than the AEI cages, indicating they are no longer in the cages of Cu-SSZ-39; however, these Cu_xO_y clusters are still believed to be stuck inside the catalysts.

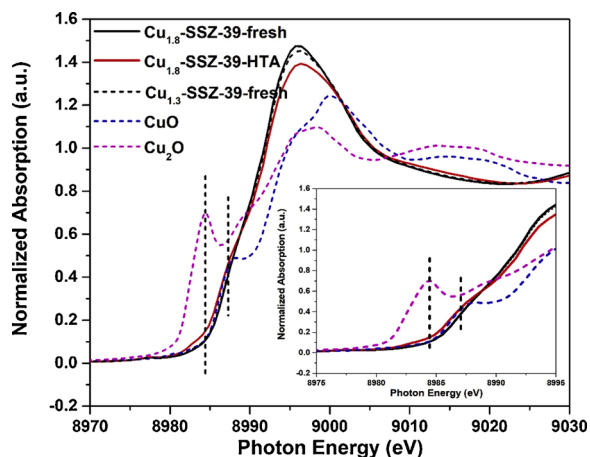


Fig. 6. XANES spectra of $\text{Cu}_{1.8}\text{-SSZ-39-fresh}$ and $\text{Cu}_{1.8}\text{-SSZ-39-HTA}$. $\text{Cu}_{1.3}\text{-SSZ-39-fresh}$, CuO and Cu_2O are presented as references.

3.4. Reaction mechanism

3.4.1. Contribution of Cu_xO_y species

In order to further investigate the contribution of Cu_xO_y species to SCR, the $\text{Cu}_{1.8}\text{-SSZ-39-fresh}$ catalyst was hydrothermally aged at various temperatures. An *in situ* DRIFTS of NH_3 adsorption experiment was used to detect changes in the amount of Cu^{2+} ions, and the results are presented in Fig. S6. It was found that the amount of Cu^{2+} ions decreases with the aging temperature, which indicates that the amount of Cu_xO_y species increases with the aging temperature. The standard SCR rates at $200/250\text{ }^\circ\text{C}$ of these catalysts aged at various temperature are presented in Fig. 8. The standard SCR rate increases with the aging temperature; in other words, the standard SCR rate increases with Cu_xO_y content. Thus, we have proved that Cu_xO_y species contribute to low-temperature deNO_x performance.

Furthermore, we tried to dissolve some Cu_xO_y species in $\text{Cu}_{1.8}\text{-SSZ-39-HTA}$ to verify whether they are the key site for deNO_x performance. The specific treatment process is presented in the experimental section. Before the NH_3 -SCR test, the catalysts were treated at $550\text{ }^\circ\text{C}$ under NH_3 -SCR conditions to get activated and decompose HNO_3 species. The Cu^{2+} contents of the HNO_3 -treated catalysts were detected by *in situ* DRIFTS of NH_3 adsorption, and the result is shown in Fig. S6. The SCR rates at $200/250\text{ }^\circ\text{C}$ of the catalysts treated by HNO_3 are presented in Fig. 8. It can be seen that after HNO_3 treatment, the SCR rate at $200\text{ }^\circ\text{C}$ and $225\text{ }^\circ\text{C}$ decreased compared to $\text{Cu}_{1.8}\text{-SSZ-39-HTA}$; however, it is still higher than $\text{Cu}_{1.8}\text{-SSZ-39-fresh}$. In the meantime, the relative Cu^{2+} content of the HNO_3 -treated catalyst was between that of $\text{Cu}_{1.8}\text{-SSZ-39-fresh}$ and $\text{Cu}_{1.8}\text{-SSZ-39-HTA}$. As a result, the conclusion can be drawn that HNO_3 treatment dissolves some of the Cu_xO_y species, resulting in a decrease in the SCR rate at $200\text{ }^\circ\text{C}$ and $225\text{ }^\circ\text{C}$ to some extent. In other words, the Cu_xO_y species in the aged catalysts are proved to be the key site for low-temperature deNO_x performance.

3.4.2. *In situ* DRIFTS experiments

To investigate the reaction mechanism over $\text{Cu}_{1.8}\text{-SSZ-39-fresh}$ and $\text{Cu}_{1.8}\text{-SSZ-39-HTA}$, a series of *in situ* DRIFTS experiments were performed. First, reaction was carried out between pre-adsorbed NH_3 and $\text{NO} + \text{O}_2$, and the results are depicted in Fig. 9. To better compare the acidity of the fresh and aged catalyst, spectra at 0 min when catalysts were saturated with NH_3 are presented in Fig. S7. The negative peaks at 3606 and 3585 cm^{-1} were assigned to the consumption of OH in Brønsted acid sites by NH_3 adsorption. The IR absorbance around $3400\text{--}3100\text{ cm}^{-1}$ was attributed to the stretching vibration of N—H bonds, and the peaks at 3326 , 3273 and 3188 cm^{-1} were assigned to NH_4^+ species [33,34]. The peaks at 1617 and 1437 cm^{-1} were assigned to the bending vibration of N—H bonds of coordinated NH_3 on Lewis acid sites and Brønsted acid sites, respectively [35,36]. Furthermore, the negative peaks around $\sim 900\text{ cm}^{-1}$ were assigned to the zeolite T—O—T vibration disrupted by Cu^{2+} , which is thoroughly discussed in Fig. S3. In the aged catalyst, the negative peaks at 3604 and 3582 cm^{-1} were much weaker than those in the fresh catalysts, indicating that the Brønsted acid sites were partly damaged by the aging process. A similar conclusion can also be drawn from the decrease in peak heights at 3335 , 3273 , 3188 and 1436 cm^{-1} , which also represent the adsorption of NH_3 on Brønsted acid sites.

The spectrum and heat map of $\text{Cu}_{1.8}\text{-SSZ-39-fresh}$ are presented in Fig. 9(a) and (b), respectively. It can be observed that the NH_3 adsorbed on both Lewis and Brønsted acid sites decreased after the introduction of $\text{NO} + \text{O}_2$. The peak at 1617 cm^{-1} corresponding to NH_3 on Lewis acid sites kept decreasing for the first 7 min, and then the intensity did not change anymore. This is because the peaks of nitrate species also emerge around this wavenumber, and stay constant after 7 min. However, it can be concluded that NH_3 adsorbed on Lewis acid sites is consumed by around 7 min. In the meantime, the peak at 1437 cm^{-1} representing NH_3 on Brønsted acid sites still existed even at 30 min. This indicated that the consumption of NH_3 on Lewis acid sites was much faster than that on

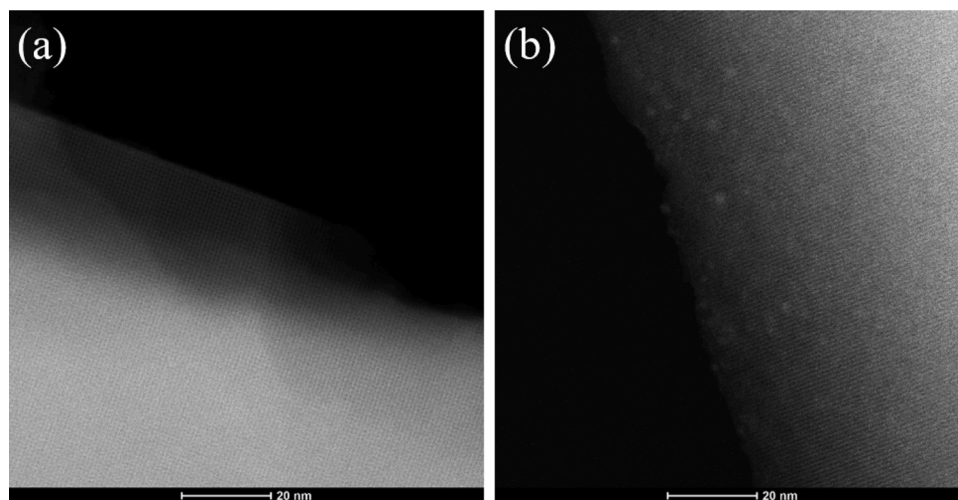


Fig. 7. TEM images of (a) $\text{Cu}_{1.8}\text{-SSZ-39-fresh}$ and (b) $\text{Cu}_{1.8}\text{-SSZ-39-HTA}$.

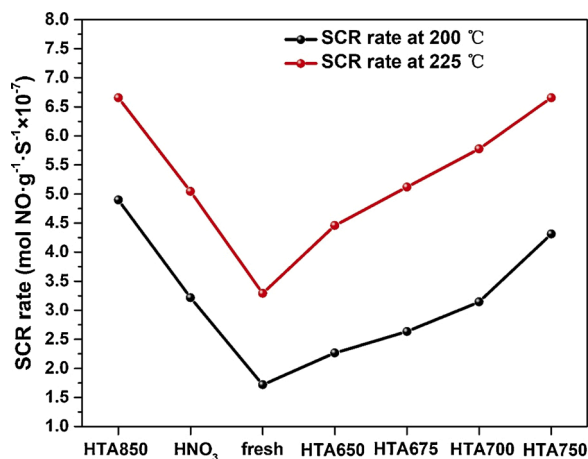


Fig. 8. The relation between SCR rate and Cu^{2+} content of Cu-SSZ-39 catalysts after hydrothermal aging at different temperatures and treatment by HNO_3 .

Brønsted acid sites. However, the trend of peak intensities was a little different for $\text{Cu}_{1.8}\text{-SSZ-39-HTA}$. As can be seen in Fig. 9(c) and (d), the peak at 1436 cm^{-1} increased after NO and O_2 were introduced. At around 4 min, this peak rose to a maximum, and then began to decrease. It is worth mentioning that apart from NH_3 adsorbed on Brønsted acid sites, the peaks for nitrate species also emerge around $1400\text{--}1500\text{ cm}^{-1}$ [25,36,37]. The increase in peak intensity around 1436 cm^{-1} could be due to the formation nitrate species on the aged catalyst. Meanwhile, the consumption of NH_3 adsorbed on Lewis acid sites was still faster than on Brønsted acid sites. However, it took a little longer for NH_3 adsorbed on Lewis acid sites to be consumed for the aged catalyst than the fresh catalyst. This phenomenon indicated that the reaction pathway may be different in $\text{Cu}_{1.8}\text{-SSZ-39-fresh}$ and $\text{Cu}_{1.8}\text{-SSZ-39-HTA}$, and that nitrate species formed more easily on the aged catalyst.

In order to further investigate the reaction process for the fresh and aged catalysts, the sequence for the introduction of gas was shifted. NO and O_2 were firstly introduced to the catalysts until saturation, and then NH_3 was introduced at 0 min after purging by N_2 . The spectra of this process are shown in Fig. S8, and for convenience of comparison, the spectra at 0 min when NO and O_2 were saturated are presented in Fig. S9. The peaks around $1500\text{--}1700\text{ cm}^{-1}$ were assigned to nitrate species adsorbed on Cu^{2+} ions, and the intensity of these peaks was stronger in $\text{Cu}_{1.8}\text{-SSZ-39-HTA}$ [25,36,37]. In the meantime, new peaks around $1300\text{--}1500\text{ cm}^{-1}$ could be observed for the aged catalyst, and

these species were attributed to bridging nitrates and ionic nitrates [38, 39]. Compared with $\text{Cu}_{1.8}\text{-SSZ-39-fresh}$, more amounts and types of nitrate species were observed in $\text{Cu}_{1.8}\text{-SSZ-39-HTA}$, indicating that nitrate species were formed more easily in $\text{Cu}_{1.8}\text{-SSZ-39-HTA}$. After NH_3 was introduced, the peaks for nitrate species disappeared and overlapped with the peaks for Lewis and Brønsted acid sites. The decrease in peaks around $1300\text{--}1700\text{ cm}^{-1}$ indicated that nitrite species can react with NH_3 , and all the nitrate species were consumed within 5 min in both the fresh and aged catalysts. These results proved that the adsorbed nitrate species can react with NH_3 at a rather rapid rate. Meanwhile, more nitrate species formed in $\text{Cu}_{1.8}\text{-SSZ-39-HTA}$, facilitating the reaction of nitrate species with NH_3 . A similar phenomenon was also observed in a recent study published by our group. We found that NH_4NO_3 species were easily formed in Cu-SSZ-39 , and they reacted with NO at a rapid rate [40]. As we observed in Fig. 9, the reaction between NH_3 adsorbed on Lewis acid sites and $\text{NO} + \text{O}_2$ was slower in $\text{Cu}_{1.8}\text{-SSZ-39-HTA}$. However, the reaction between adsorbed nitrate species and NH_3 was faster on the aged catalysts, and this process was probably why the aged catalyst performed better in $\text{NH}_3\text{-SCR}$ than the fresh one. Further discussions on the $\text{NH}_3\text{-SCR}$ pathway of the two catalysts will be included in the next section.

4. Discussion

4.1. Abnormal hydrothermal aging effect

As we mentioned in the introduction section, it is quite abnormal that the catalytic activity of these small pore zeolites improved after hydrothermal aging. Fickel et al. were the first to find that after hydrothermal aging, the $\text{NH}_3\text{-SCR}$ performance of Cu-SAPO-34 was improved [14]. Wang et al. further investigated this phenomenon, and found that the migration of Cu_xO_y clusters on the surface of the catalyst into active Cu^{2+} species resulted in the increase of catalytic activity [16]. Afterwards, similar circumstances were observed in numbers of studies, and the same conclusion was drawn [2,15,41]. Furthermore, an increase in $\text{NH}_3\text{-SCR}$ activity after hydrothermal aging was also observed in Cu-LTA zeolites by Hong and Nam et al. During the aging process, Cu^+ migrated from sod cages into single 6-rings, along with the oxidation of Cu^+ into Cu^{2+} , which resulted in the improvement of catalytic performance [17,42]. However, the circumstance was quite different in Cu-SSZ-39 . Through the investigations on Cu species over $\text{Cu}_{1.8}\text{-SSZ-39-fresh}$ and $\text{Cu}_{1.8}\text{-SSZ-39-HTA}$, the conclusion was drawn that the formation of Cu_xO_y species contributed to the increase in low-temperature catalytic activity after hydrothermal aging. In the study of ZSM-5 , Pereda-Ayo et al. found that Cu_xO_y species oxidized NO

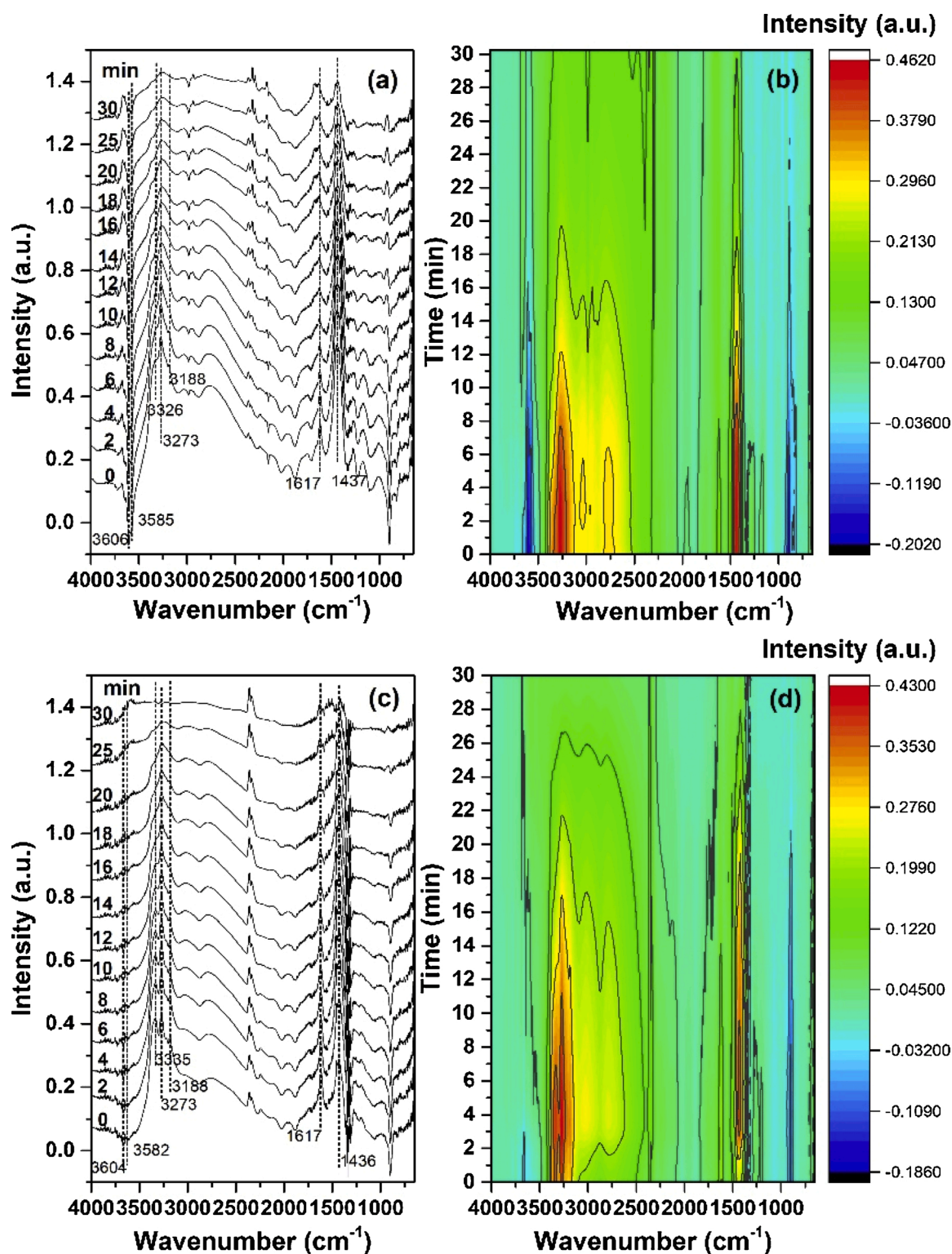


Fig. 9. (a) *In situ* DRIFTS spectra and (b) heat map of $\text{Cu}_{1.8}\text{-SSZ-39-fresh}$ exposed to $\text{NO} + \text{O}_2$ after being saturated by NH_3 . (c) *In situ* DRIFTS spectra and (d) heat map of $\text{Cu}_{1.8}\text{-SSZ-39-HTA}$ exposed to $\text{NO} + \text{O}_2$ after being saturated by NH_3 .

into NO_2 , which favored the low-temperature $\text{NH}_3\text{-SCR}$ activity [43]. Nevertheless, no NO_2 was observed in the oxidation of NO in this study, neither in $\text{Cu}_{1.8}\text{-SSZ-39-fresh}$ nor in $\text{Cu}_{1.8}\text{-SSZ-39-HTA}$. As a result, the function of Cu_xO_y species in Cu-SSZ-39 was different from that in Cu-ZSM-5 , which will be thoroughly demonstrated in the following sections.

It is worth mentioning that the catalytic activity of Cu-SSZ-39 with

very low or high Cu loading was not improved after hydrothermal aging. As presented in Fig. S1, the catalytic activity of $\text{Cu}_{0.5}\text{-SSZ-39-fresh}$ increased with rising temperature, and no “seagull shape” profile was observed. In the study of Cu-SSZ-13 , a “seagull shape” profile existed in $\text{NH}_3\text{-SCR}$ tests when Cu loading was low [13,20,21]. Under $\text{NH}_3\text{-SCR}$ conditions, NH_3 coordinates with Cu ions in the low-temperature range, which facilitates the mobility of Cu ions. Therefore, Cu ions can move

among zeolite cages, forming transient Cu dimers, which activate O₂ in the oxidation of Cu⁺ into Cu²⁺ [44–46]. When the temperature rises to around 350 °C, NH₃ becomes detached from Cu ions, and Cu⁺/Cu²⁺ anchor to the ion-exchanged sites, becoming active centers for the reaction. NH₃-SCR rate decreases without the good mobility of Cu ions. When the temperature further rises, the effective collision probability of reactant molecules increases; as a consequence, the catalytic activity rises again. However, in Cu_{0.5}-SSZ-39-fresh, the standard SCR rate was very low from 150 °C to 350 °C. This was probably due to the content of Cu being so low that the Cu ions could not meet each other to combine into pairs even with the help of NH₃. From another prospective, Cu_xO_y species could hardly form during the hydrothermal aging process due to the deficiency of Cu ions, so that the catalytic activity was not improved. Furthermore, we also found that Cu ions could help to stabilize framework atoms during the hydrothermal aging process [26]. However, if the Cu loading was too high, Cu_xO_y clusters would form, which facilitated the deterioration of the framework [12]. The XRD profiles of the fresh and aged catalysts with Cu loading of 0.5 % and 2.3 % are presented in Fig. S10. The crystallinity of Cu_{0.5}-SSZ-39-HTA showed little change compared with Cu_{0.5}-SSZ-39-fresh; however, a remarkable decrease in crystallinity was observed in Cu_{2.3}-SSZ-39-HTA, indicating that the framework was affected by the hydrothermal aging process. The same phenomenon was more obvious in a Cu_{3.5}-SSZ-39 catalyst in our previous study with much higher Cu loading [3]. This result indicated that excessive Cu ions existed in Cu_{2.3}-SSZ-39, leading to Cu_xO_y clusters being formed and damaging the skeleton. As a result, the catalytic activity of Cu_{0.5}-SSZ-39-HTA and Cu_{2.3}-SSZ-39-HTA was lower than the fresh catalysts.

4.2. Function of Cu_xO_y species in Cu-SSZ-39

Cu_xO_y species have generally not been recognized as active sites for NH₃-SCR in small-pore zeolites, and they were believed to do harm to the high-temperature catalytic activity due to the non-selective catalytic oxidation of NH₃ [8,9]. However, different points of view were also held by some other researchers. In the study of Cu-SAPO-34, Weng et al. observed that the low-temperature catalytic activity decreased while the high-temperature NO_x conversion improved after hydrothermal aging. Through the investigation of Cu species, it was discovered that the conversion of Cu_xO_y species into Cu²⁺ species resulted in this phenomenon, and they concluded that Cu_xO_y species were beneficial to low-temperature catalytic activity [47]. With the help of DFT theoretical calculations, [Cu-O-Cu]²⁺ species inside CHA cages were also proved to be active centers for NH₃-SCR in Cu-SAPO-34 by Du et al. [48]. Furthermore, Grunwaldt et al. investigated the NH₃-SCR mechanism over Cu-SSZ-13 with low and high Cu loading. A conclusion was drawn that dimeric Cu⁺-O₂-Cu⁺ species formed in highly loaded catalysts, relating to the good low-temperature catalytic activity [49].

In this study, we have also proved that Cu_xO_y species are NH₃-SCR active in Cu-SSZ-39. As a result, we need to reexamine the function of Cu_xO_y species in NH₃-SCR over small-pore zeolites. The whole NH₃-SCR process in small-pore zeolites can be recognized as a redox cycle of Cu⁺ and Cu²⁺ ions. In the reduction half-cycle of Cu²⁺ into Cu⁺, NO and NH₃ co-activate Cu²⁺, resulting in the formation of N₂ and H₂O. In the oxidation half cycle, two Cu⁺ coordinated with NH₃ migrate into one cage to activate O₂, forming transient Cu-dimers which further react with NO when Cu loading is low. Due to the electrostatic tethering to skeleton Al atoms, the formation of [Cu^I(NH₃)₂]⁺-O₂-[Cu^I(NH₃)₂]⁺ intermediates is the rate-limiting step. However, things are different when Cu loading is high. Cu_xO_y species formed when catalysts were highly loaded, and the formed Cu_xO_y species facilitated the low-temperature SCR performance [21,49]. In this study, hydrothermal aging treatment created Cu_xO_y species in Cu-SSZ-39, and these Cu_xO_y species act as active centers. The hydrothermal aging process induces the formation of Cu_xO_y species even when the Cu loading is not very high, so that the aged catalysts can perform as well as the catalysts with high Cu loading.

This process can be proved by the standard SCR rate profile of the aged catalysts in that no “seagull shape” profile was observed in the aged catalysts, whatever the Cu loading. As we discussed above, the reason for the “seagull shape” was due to the change in the reaction mechanism around 350 °C. With the formation of Cu_xO_y species, the migration of Cu⁺ ions through cages no longer restricts the deNO_x performance in the low-temperature range, leading to the disappearance of the “seagull shape”. To sum up, the hydrothermal aging process created active Cu_xO_y species, so that the low-temperature catalytic activity was improved.

Furthermore, it is quite interesting to notice that it has never been reported that the hydrothermal aging process could facilitate the low-temperature catalytic activity of Cu-SSZ-13. This is due to the structural differences between Cu-SSZ-13 and Cu-SSZ-39. In a previous study by our group, we compared the hydrothermal stability of Cu-SSZ-13 and Cu-SSZ-39. The better hydrothermal stability of Cu-SSZ-39 was due to the fact that more paired framework Al atoms were found in Cu-SSZ-39, which resulted in the formation of more hydrothermally stable Cu²⁺ species. Furthermore, the channels in Cu-SSZ-39 are more tortuous, which hinders the detachment of framework Al atoms [3]. As we reached a deeper understanding of the inactivation mechanism after hydrothermal aging, researchers found that the formation of CuAlO_x species, rather than Cu_xO_y, was the real reason that small-pore zeolites lose catalytic activity [9,50]. Compared with Cu-SSZ-39, CuAlO_x species formed more easily in Cu-SSZ-13 due to the framework instability; as a consequence, the catalytic activity was never promoted in Cu-SSZ-13 after hydrothermal aging. From another aspect, the promotion effect of Cu_xO_y species on the catalytic activity of Cu-SSZ-13 may not be as obvious as that of Cu-SSZ-39. The CHA structure is very beneficial to the mobility of Cu(NH₃)_x, resulting in excellent catalytic activity, while the AEI structure with more tortuous channels inhibits the migration of Cu(NH₃)_x⁺ ions. As a result, the low-temperature catalytic activity of the fresh Cu-SSZ-39 catalyst was lower than that of Cu-SSZ-13 [3]. The small Cu_xO_y clusters are more active than Cu²⁺ ions in Cu-SSZ-39, so that the formation of these Cu_xO_y clusters contributed greatly to the low-temperature catalytic activity. As a result, improvement of the low-temperature catalytic activity after hydrothermal aging was observed in Cu-SSZ-39 but not Cu-SSZ-13.

5. Conclusion

Due to the regeneration of DPF, hydrothermal aging is inevitable for SCR catalysts in heavy-duty diesel vehicles. Unlike typical NH₃-SCR catalysts, we found an unexpected increase in the low-temperature NH₃-SCR catalytic activity over Cu-SSZ-39 with moderate Cu content after hydrothermal aging. During the aging process, dealumination of SSZ-39 only slightly occurred and a portion of the Cu²⁺ accumulated to form Cu_xO_y species. The formation of Cu_xO_y species facilitated the formation of nitrate species, which bypassed the rate-determining step of migration of Cu⁺ species to activate O₂ and NO, resulting in the unexpected improvement of SCR activity. Moreover, only the Cu-SSZ-39 catalysts with suitable Cu contents (1.3–2.0 wt.%) could be improved in this way, while both too little and too much Cu caused deterioration of NH₃-SCR activity of Cu-SSZ-39 after hydrothermal aging. Cu-SSZ-39 is already known for its exceptional hydrothermal stability and the new finding of the increase of catalytic activity after hydrothermal aging provides further potential for the actual application of Cu-SSZ-39 for the removal of NO_x from diesel exhaust.

CRedit authorship contribution statement

Jinpeng Du: Data curation, Investigation, Formal analysis, Writing - original draft, Writing - review & editing. **Yulong Shan:** Conceptualization, Methodology, Validation, Writing - review & editing, Project administration. **Yu Sun:** Data curation, Investigation, Validation. **Meng Gao:** Data curation, Investigation, Validation. **Zhongqi Liu:** Data curation, Investigation, Validation. **Xiaoyan Shi:** Conceptualization,

Methodology, Validation. **Yunbo Yu**: Conceptualization, Methodology, Validation. **Hong He**: Conceptualization, Writing - review & editing, Project administration, Resources, Supervision.

Declaration of Competing Interest

The authors declare that they have no known competing financial interests or personal relationships that could have appeared to influence the work reported in this paper.

Acknowledgments

This work was financially supported by the National Natural Science Foundation of China (21906172, 21637005) and Ozone Formation Mechanism and Control Strategies Project of Research Center for Eco-Environmental Sciences, CAS (RCEES-CYZX-2020). We thank the 1W1B beamline of Beijing Synchrotron Radiation Facility for their support of the XAFS experiments.

Appendix A. Supplementary data

Supplementary material related to this article can be found, in the online version, at doi:<https://doi.org/10.1016/j.apcatb.2021.120237>.

References

- Y. Shan, J. Du, Y. Zhang, W. Shan, X. Shi, Y. Yu, R. Zhang, X. Meng, F.-S. Xiao, H. He, Selective catalytic reduction of NO_x with NH₃: opportunities and challenges of Cu-based small-pore zeolites, *Natl. Sci. Rev.* 8 (2021), <https://doi.org/10.1093/nsr/nwab010>.
- D. Wang, Y. Jangjou, Y. Liu, M.K. Sharma, J. Luo, J. Li, K. Kamasamudram, W. S. Epling, A comparison of hydrothermal aging effects on NH₃-SCR of NO_x over Cu-SSZ-13 and Cu-SAPO-34 catalysts, *Appl. Catal. B* 165 (2015) 438–445.
- Y. Shan, W. Shan, X. Shi, J. Du, Y. Yu, H. He, A comparative study of the activity and hydrothermal stability of Al-rich Cu-SSZ-39 and Cu-SSZ-13, *Appl. Catal. B* 264 (2020) 118511–118520.
- J. Du, Y. Shan, G. Xu, Y. Sun, Y. Wang, Y. Yu, W. Shan, H. He, Effects of SO₂ on Cu-SSZ-39 catalyst for the selective catalytic reduction of NO_x with NH₃, *Catal. Sci. Technol.* 10 (2020) 1256–1263.
- H. Xu, W. Chen, Q. Wu, C. Lei, J. Zhang, S. Han, L. Zhang, Q. Zhu, X. Meng, D. Dai, S. Maurer, A.-N. Parvulescu, U. Müller, W. Zhang, T. Yokoi, X. Bao, B. Marler, D. E. De Vos, U. Kolb, A. Zheng, F.-S. Xiao, Transformation synthesis of aluminosilicate SSZ-39 zeolite from ZSM-5 and beta zeolite, *J. Mater. Chem. A* 7 (2019) 4420–4425.
- X. Ye, J.E. Schmidt, R.P. Wang, I.K. van Ravenhorst, R. Oord, T. Chen, F. de Groot, F. Meirer, B.M. Weckhuysen, Deactivation of Cu-Exchanged automotive-emission NH₃-SCR catalysts elucidated with nanoscale resolution using scanning transmission X-ray microscopy, *Angew. Chem. Int. Ed. Engl.* 132 (2020) 15740–15747.
- Y.J. Kim, J.K. Lee, K.M. Min, S.B. Hong, I.-S. Nam, B.K. Cho, Hydrothermal stability of Cu-SSZ-13 for reducing NO_x by NH₃, *J. Catal.* 311 (2014) 447–457.
- Y. Shan, J. Du, Z. Yan, Y. Yu, H. He, SSZ-13 synthesized by solvent-free method: a potential candidate for NH₃-SCR catalyst with high activity and hydrothermal stability, *Ind. Eng. Chem. Res.* 58 (2019) 5397–5403.
- Yue Ma, X. Wu, S. Cheng, L. Cao, L. Liu, Y. Xu, J. Liu, R. Ran, Z. Si, D. Weng, Relationships between copper speciation and Brønsted acidity evolution over Cu-SSZ-13 during hydrothermal aging, *Appl. Catal. A* 602 (2020) 117650–117661.
- H. Kubota, C. Liu, T. Toyao, Z. Maeno, M. Ogura, N. Nakazawa, S. Inagaki, Y. Kubota, K. Shimizu, Formation and reactions of NH₄NO₃ during transient and SteadyState NH₃-SCR of NO_x over H-AFX zeolites: spectroscopic and theoretical studies, *ACS Catal.* 10 (2020) 2334–2344.
- S. Li, Y. Zheng, F. Gao, J. Szanyi, W.F. Schneider, Experimental and computational interrogation of fast SCR mechanism and active sites on H-Form SSZ-13, *ACS Catal.* 7 (2017) 5087–5096.
- J. Song, Y. Wang, E.D. Walter, N.M. Washton, D. Mei, L. Kovarik, M.H. Engelhard, S. Proding, Y. Wang, C.H.F. Peden, F. Gao, Toward rational design of Cu/SSZ-13 selective catalytic reduction catalysts: implications from atomic-level understanding of hydrothermal stability, *ACS Catal.* 7 (2017) 8214–8227.
- F. Gao, C.H.F. Peden, Recent progress in atomic-level understanding of Cu/SSZ-13 selective catalytic reduction catalysts, *Catalysts* 8 (2018) 140–162.
- D.W. Fickel, E. D'Addio, J.A. Lauterbach, R.F. Lobo, The ammonia selective catalytic reduction activity of copper-exchanged small-pore zeolites, *Appl. Catal. B* 102 (2011) 441–448.
- J. Du, Y. Shan, W. Zhang, Y. Yu, W. Shan, H. He, Investigation of suitable templates for one-pot-synthesized CuSAPO-34 in NO_x abatement from diesel vehicle exhaust, *Environ. Sci. Technol.* 54 (2020) 7870–7878.
- L. Wang, J.R. Gaudet, W. Li, D. Weng, Migration of Cu species in Cu/SAPO-34 during hydrothermal aging, *J. Catal.* 306 (2013) 68–77.
- D. Jo, T. Ryu, G.T. Park, P.S. Kim, C.H. Kim, I.-S. Nam, S.B. Hong, Synthesis of high-silica LTA and UFI zeolites and NH₃-SCR performance of their copper-exchanged form, *ACS Catal.* 6 (2016) 2443–2447.
- T. Ryu, N.H. Ahn, S. Seo, J. Cho, H. Kim, D. Jo, G.T. Park, P.S. Kim, C.H. Kim, E. L. Bruce, P.A. Wright, I.S. Nam, S.B. Hong, Fully copper-exchanged high-silica LTA zeolites as unrivaled hydrothermally stable NH₃-SCR catalysts, *Angew. Chem. Int. Ed. Engl.* 56 (2017) 3256–3260.
- T. Sonoda, T. Maruo, Y. Yamasaki, N. Tsumoji, Y. Takamitsu, M. Sadakane, T. Sano, Synthesis of high-silica AEI zeolites with enhanced thermal stability by hydrothermal conversion of FAU zeolites, and their activity in the selective catalytic reduction of NO_x with NH₃, *J. Mater. Chem. A* 3 (2015) 857–865.
- F. Gao, E.D. Walter, M. Kollar, Y. Wang, J. Szanyi, C.H.F. Peden, Understanding ammonia selective catalytic reduction kinetics over Cu/SSZ-13 from motion of the Cu ions, *J. Catal.* 319 (2014) 1–14.
- F. Gao, D. Mei, Y. Wang, J. Szanyi, C.H. Peden, Selective catalytic reduction over Cu/SSZ-13: linking homo- and heterogeneous catalysis, *J. Am. Chem. Soc.* 139 (2017) 4935–4942.
- F. Gao, E.D. Walter, E.M. Karp, J. Luo, R.G. Tonkyn, J.H. Kwak, J. Szanyi, C.H. F. Peden, Structure–activity relationships in NH₃-SCR over Cu-SSZ-13 as probed by reaction kinetics and EPR studies, *J. Catal.* 300 (2013) 20–29.
- Y. Wang, X. Shi, Y. Shan, J. Du, K. Liu, H. He, Hydrothermal stability enhancement of Al-Rich Cu-SSZ-13 for NH₃ selective catalytic reduction reaction by ion exchange with cerium and samarium, *Ind. Eng. Chem. Res.* 59 (2020) 6416–6423.
- L. Xie, F. Liu, X. Shi, F.-S. Xiao, H. He, Effects of post-treatment method and Na cation on the hydrothermal stability of Cu-SSZ-13 catalyst for the selective catalytic reduction of NO_x with NH₃, *Appl. Catal. B* 179 (2015) 206–212.
- Y. Shan, J. Du, Y. Zhang, X. Shi, Y. Yu, W. Shan, H. He, Hydrothermal aging alleviates the inhibition effects of NO₂ on Cu-SSZ-13 for NH₃-SCR, *Appl. Catal. B* 275 (2020) 119105–119114.
- Y. Shan, J. Du, Y. Yu, W. Shan, X. Shi, H. He, Precise control of post-treatment significantly increases hydrothermal stability of in-situ synthesized Cu-zeolites for NH₃-SCR reaction, *Appl. Catal. B* 266 (2020) 118655–118666.
- Z. Chen, C. Fan, L. Pang, S. Ming, P. Liu, T. Li, The influence of phosphorus on the catalytic properties, durability, sulfur resistance and kinetics of Cu-SSZ-13 for NO_x reduction by NH₃-SCR, *Appl. Catal. B* 237 (2018) 116–127.
- Z. Zhao, R. Yu, R. Zhao, C. Shi, H. Gies, F.-S. Xiao, D. De Vos, T. Yokoi, X. Bao, U. Kolb, M. Feyen, R. McGuire, S. Maurer, A. Moini, U. Müller, W. Zhang, Cu-exchanged Al-rich SSZ-13 zeolite from organotemplate-free synthesis as NH₃-SCR catalyst: effects of Na⁺ ions on the activity and hydrothermal stability, *Appl. Catal. B* 217 (2017) 421–428.
- S. Han, Q. Ye, S. Cheng, T. Kang, H. Dai, Effect of the hydrothermal aging temperature and Cu/Al ratio on the hydrothermal stability of CuSSZ-13 catalysts for NH₃-SCR, *Catal. Sci. Technol.* 7 (2017) 703–717.
- S.A. Bates, A.A. Verma, C. Paolucci, A.A. Parekh, T. Anggara, A. Yezerets, W. F. Schneider, J.T. Miller, W.N. Delgass, F.H. Ribeiro, Identification of the active Cu site in standard selective catalytic reduction with ammonia on Cu-SSZ-13, *J. Catal.* 312 (2014) 87–97.
- K. Leistner, K. Xie, A. Kumar, K. Kamasamudram, L. Olsson, Ammonia desorption peaks can be assigned to different copper sites in Cu/SSZ-13, *Catal. Lett.* 147 (2017) 1882–1890.
- R. Li, Y. Zhu, Z. Zhang, C. Zhang, G. Fu, X. Yi, Q. Huang, F. Yang, W. Liang, A. Zheng, J. Jiang, Remarkable performance of selective catalytic reduction of NO_x by ammonia over copper-exchanged SSZ-52 catalysts, *Appl. Catal. B* 283 (2021) 119641–119650.
- D. Wang, L. Zhang, K. Kamasamudram, W.S. Epling, In Situ-DRIFTS study of selective catalytic reduction of NO_x by NH₃ over Cu-Exchanged SAPO-34, *ACS Catal.* 3 (2013) 871–881.
- L. Xie, F. Liu, K. Liu, X. Shi, H. He, Inhibitory effect of NO₂ on the selective catalytic reduction of NO_x with NH₃ over one-pot-synthesized Cu-SSZ-13 catalyst, *Catal. Sci. Technol.* 4 (2014) 1104–1110.
- H. Zhu, J.H. Kwak, C.H.F. Peden, J. Szanyi, In situ DRIFTS-MS studies on the oxidation of adsorbed NH₃ by NO_x over a Cu-SSZ-13 zeolite, *Catal. Today* 205 (2013) 16–23.
- Y. Zhang, Y. Peng, K. Li, S. Liu, J. Chen, J. Li, F. Gao, C.H.F. Peden, Using transient FTIR spectroscopy to probe active sites and reaction intermediates for selective catalytic reduction of NO on Cu/SSZ-13 catalysts, *ACS Catal.* 9 (2019) 6137–6145.
- Y. Ma, S. Cheng, X. Wu, Y. Shi, L. Cao, L. Liu, R. Ran, Z. Si, J. Liu, D. Weng, Low-temperature solid-state ion-exchange method for preparing Cu-SSZ-13 selective catalytic reduction catalyst, *ACS Catal.* 9 (2019) 6962–6973.
- D. Meng, Q. Xu, Y. Jiao, Y. Guo, Y. Guo, L. Wang, G. Lu, W. Zhan, Spinel structured Co_{0.4}Mn_{0.6}O_x mixed oxide catalyst for the selective catalytic reduction of NO_x with NH₃, *A Appl. Catal. B* 221 (2018) 652–663.
- Q. Li, M. Meng, Z.Q. Zou, X.G. Li, Y.Q. Zha, Simultaneous soot combustion and nitrogen oxides storage on potassium-promoted hydrothermalite-based CoMgAlO catalysts, *J. Hazard. Mater.* 161 (2009) 366–372.
- N. Zhu, Y. Shan, W. Shan, Y. Sun, K. Liu, Y. Zhang, H. He, Distinct NO₂ effects on Cu-SSZ-13 and Cu-SSZ-39 in the selective catalytic reduction of NO_x with NH₃, *Environ. Sci. Technol.* 54 (2020) 15499–15506.
- J. Wang, Y. Huang, T. Yu, S. Zhu, M. Shen, W. Li, J. Wang, The migration of Cu species over Cu-SAPO-34 and its effect on NH₃ oxidation at high temperature, *Catal. Sci. Technol.* 4 (2014) 3004–3012.
- N.H. Ahn, T. Ryu, Y. Kang, H. Kim, J. Shin, I.-S. Nam, S.B. Hong, The origin of an unexpected increase in NH₃-SCR activity of aged Cu-LTA catalysts, *ACS Catal.* 7 (2017) 6781–6785.

- [43] B. Pereda-Ayo, U. De La Torre, M.J. Illán-Gómez, A. Bueno-López, J.R. González-Velasco, Role of the different copper species on the activity of Cu/zeolite catalysts for SCR of NO_x with NH₃, *Appl. Catal. B* 147 (2014) 420–428.
- [44] C. Paolucci, I. Khurana, A.A. Parekh, A.J. Shih, H. Li, J.R.D. Iorio, J.D. Albarracín-Caballero, A. Yezerets, J.T. Miller, W.N. Delgass, F.H. Ribeiro, W.F. Schneider, R. Gounder, Dynamic multinuclear sites formed by mobilized copper ions in NO_x selective catalytic reduction, *Science* 357 (2017) 858–903.
- [45] C. Paolucci, A.A. Parekh, I. Khurana, J.R. Di Iorio, H. Li, J.D.A. Caballero, A. J. Shih, T. Anggara, W.N. Delgass, J.T. Miller, F.H. Ribeiro, R. Gounder, W. F. Schneider, Catalysis in a cage: condition-dependent speciation and dynamics of exchanged Cu cations in SSZ-13 zeolites, *J. Am. Chem. Soc.* 138 (2016) 6028–6048.
- [46] P. Chen, A. Khetan, M. Jabłońska, J. Simböck, M. Muhler, R. Palkovits, H. Pitsch, U. Simon, Local dynamics of copper active sites in zeolite catalysts for selective catalytic reduction of NO_x with NH₃, *Appl. Catal. B* 237 (2018) 263–272.
- [47] X. Liu, X. Wu, D. Weng, Z. Si, R. Ran, Evolution of copper species on Cu/SAPO-34 SCR catalysts upon hydrothermal aging, *Catal. Today* 281 (2017) 596–604.
- [48] G. Yang, J. Ran, X. Du, X. Wang, Y. Chen, L. Zhang, Different copper species as active sites for NH₃-SCR reaction over Cu-SAPO-34 catalyst and reaction pathways: a periodic DFT study, *Microporous Mesoporous Mater.* 266 (2018) 223–231.
- [49] A.R. Fahami, T. Günter, D.E. Doronkin, M. Casapu, D. Zengel, T.H. Vuong, M. Simon, F. Breher, A.V. Kucherov, A. Brückner, J.D. Grunwaldt, The dynamic nature of Cu sites in Cu-SSZ-13 and the origin of the seagull NO_x conversion profile during NH₃-SCR, *React. Chem. Eng.* 4 (2019) 1000–1018.
- [50] A. Wang, Y. Chen, E.D. Walter, N.M. Washton, D. Mei, T. Varga, Y. Wang, J. Szanyi, Y. Wang, C.H.F. Peden, F. Gao, Unraveling the mysterious failure of Cu/SAPO-34 selective catalytic reduction catalysts, *Nat. Commun.* 10 (2019) 1137–1146.